JPE 16-4-21

http://dx.doi.org/10.6113/JPE.2016.16.4.1455
ISSN(Print): 1598-2092 / ISSN(Online): 2093-4718

Grid-Connected Dual Stator-Winding Induction Generator Wind Power System for Wide Wind Speed Ranges

Kai Shi[†], Peifeng Xu[*], Zengqiang Wan[*], Feifei Bu[**], Zhiming Fang[*], Rongke Liu[***], and Dean Zhao[*]

[†,*]School of Electrical and Information Engineering, Jiangsu University, Zhenjiang, China
[**]College of Automation Engineering, Nanjing University of Aeronautics and Astronautics, Nanjing, China
[***]KTK Group, Changzhou, China

Abstract

This paper presents a grid-connected dual stator-winding induction generator (DWIG) wind power system suitable for wide wind speed ranges. The parallel connection via a unidirectional diode between dc buses of both stator-winding sides is employed in this DWIG system, which can output a high dc voltage over wide wind speed ranges. Grid-connected inverters (GCIs) do not require booster converters; hence, the efficiency of wind energy utilization increases, and the hardware topology and control strategy of GCIs are simplified. In view of the particularities of the parallel topology and the adopted generator control strategy, we propose a novel excitation–capacitor optimization solution to reduce the volume and weight of the static excitation controller. When this excitation–capacitor optimization is carried out, the maximum power tracking problem is also considered. All the problems are resolved with the combined control of the DWIG and GCI. Experimental results on the platform of a 37 kW/600 V prototype show that the proposed DWIG wind power system can output a constant dc voltage over wide rotor speed ranges for grid-connected operations and that the proposed excitation optimization scheme is effective.

Key words: Dual stator-winding induction generator (DWIG), Excitation–capacitor optimization, Grid connection, Wind power, Wide wind speed

I. INTRODUCTION

Since the beginning of the 21st century, wind energy has become one of the most important ways to address the energy crisis. Wind energy offers several advantages, including a vast quantity, a wide regional distribution, and zero pollution generation. Although commonly used, the direct-drive permanent magnet synchronous generator (PMSG) and doubly fed induction generator (DFIG) wind turbines possess inherent disadvantages [1]. The PMSG wind turbine is made expensive by its rare permanent magnetic material, and its direct-drive structure is bulky and heavy. The DFIG requires brushes and copper rings for the power transfer to and from rotor windings and thus entails high maintenance costs [2].

As a novel induction generator proposed at the beginning of this century, the dual stator-winding induction generator (DWIG) not only inherits some advantages of conventional induction generators (IGs), such as robust brushless construction, low maintenance cost, and favorable overload protection [3], [4], but also overcomes its inherent drawbacks of poor voltage regulation with load and rotor speed variations [5], [6]. The lack of electrical connection between two sets of stator windings makes the DWIG exhibit a high-quality control performance under variations in speed and load. A pulse width modulation (PWM)-controlled static excitation controller (SEC) connected to a control winding is employed to provide variable compensating reactive power and thereby regulate the magnitude of the output voltage and load frequency effectively [7]. At the same time, the harmonics induced by the applied power converter connected

Manuscript received Sep. 15, 2015; accepted Feb. 14, 2016
Recommended for publication by Associate Editor Dong-Myung Lee.
[†]Corresponding Author: shikai80614@163.com
Tel: +86-0511-88791245, Jiangsu University
[*]School of Electrical and Information Engineering, Jiangsu University, China
[**]College of Automation Engineering, Nanjing University of Aeronautics and Astronautics, China
[***]KTK Group, China

in series or parallel to the load in a conventional IG system can be minimized and even eliminated [6], [7]. In recent years, the research on the DWIG for standalone power system applications has revealed its excellent static and dynamic performance [7], [8]. With the increasing need for offshore wind farms [9], [10], DWIG-based power generation systems have been proposed for high-voltage dc transmission in offshore wind farms [11], [12].

The optimal design of the DWIG structure is suitable for operations in medium- to low-speed regions. Thus, the need for an expensive and high-maintenance high-speed gearbox in DFIG wind turbines is eliminated. The favorable capability of the DWIG to operate in flux-weakening regions broadens the operational speed range of this generator. Given that the ac capacitor bank on the power winding provides reactive power and reduces the inductance of the rectifier load, the bank can be optimized to maintain the control-winding current at a minimum level and thereby decrease the capacity of the SEC [8], [10], [13]. Thus, DWIG wind power systems are excellent alternatives to conventional wind turbines.

However, wind energy varies with the time of the day, month, or season. A significant portion of the annual gross electricity production of wind turbines depends on the available wind speed range. For this reason, the research on wind energy is focused on improving wind energy extraction and extending the operating wind speed ranges of wind turbines, especially in barren areas. As a result of the limitation of the cost of wind turbine systems and the capacity of excitation converters, the direct-drive PMSG and DFIG are deemed costly for extending operating wind speed ranges. For the direct-drive PMSG wind turbine, an expensive high-gain boost converter is necessary for the high dc voltage under low wind speeds for stable grid-connected operations. As wind speed falls, the DFIG reverts to a conventional IG operation mode, with the total electric power flowing from the rotor-side converter to the grid. Hence, the capacity of the rotor-side excitation converter restricts the actual adaptive wind speed range of the DFIG. A particular control strategy for specific wind turbines and modified maximum power tracking strategies have been proposed to expand the operating ranges of wind turbines and increase their output power, especially in areas with low wind speeds [14], [15].

As a response to this problem, the topology of DWIG-based wind power systems was improved to enhance their unsatisfactory wind energy utilization in low wind speed regions [16]. To maximize wind energy, both sides of a dc bus were connected in parallel using a diode. A control-winding-flux-orientation control strategy for the DWIG and an efficiency optimization scheme in the low-speed range were subsequently presented in [16], in which different control strategies for low and high wind speeds were provided to ensure a stable high dc output voltage over wide wind speed ranges. However, the topology of grid-connected inverters (GCIs) or the grid-connected operation control strategy utilized in the study and the optimization of the excitation capacitor in a parallel topology for grid-connected operations were not investigated [16]. The particular topology of a parallel connection between two dc bus sides results in an entirely different active and reactive current component in low and high wind speed regions. Therefore, the excitation optimization scheme should be designed and reconfirmed for an improved system topology and grid-connection operation. Furthermore, the maximum power tracking problem should be considered when excitation capacitances are optimized.

In the present work, a grid-connected DWIG system for wind energy generation applications is explored. The topology of the parallel connection between two dc bus sides is still employed to output a stable high dc voltage in a wide wind speed range. As a result of the advantageous parallel topology, the booster converter is removed in the hardware structure of the GCI for the grid-connected operation. The removal of the booster converter is an outstanding advantage of the proposed grid-connected DWIG wind turbine. The different compositions of active and reactive currents in low and high wind speed ranges are considered when the capacity of the SEC is optimized while the maximum power tracking requirement is satisfied. An appropriate control strategy for a GCI without a booster converter is presented. This work is verified by the experimental results based on the prototype of a grid-connected DWIG wind turbine.

The rest of this paper is organized as follows. In Section II, a system structure diagram of the proposed grid-connected DWIG wind power system is introduced, and the operational principle is discussed in detail. In Section III, the corresponding and integrated control strategies for the proposed grid-connected DWIG wind power system for wide speed ranges are presented. In Section IV, the optimization scheme for the excitation capacitors and the simulation verification are shown. Finally, in Sections V and VI, the experimental results and conclusions are provided, respectively.

II. GRID-CONNECTED DWIG WIND POWER SYSTEM AND OPERATIONAL PRINCIPLES

The structure diagram of the proposed grid-connected DWIG wind power system is shown in Fig. 1. The first-order step-up gearbox is built to deliver mechanical energy from the wind machine to the generator. The DWIG consists of a standard squirrel-cage brushless rotor and a stator with two separate three-phase star windings wound by a 30° electrical angle shift. The power winding is linked to ac excitation capacitors and a rectifier bridge. A filter induction between the control winding and SEC is adopted to minimize

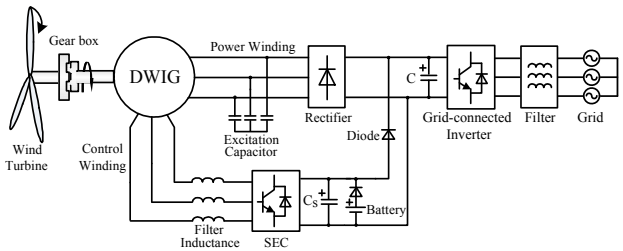

Fig. 1. Structural diagram of the proposed grid-connected DWIG wind power system.

SEC-induced harmonics. The dc bus of the SEC is connected to the dc filter capacitor. The storage battery is isolated from the high dc voltage through a diode, which contributes to the excitation at the beginning of voltage build-up. The dc buses on the control side and those on the power side are connected in parallel via the diode. The positive dc bus terminal of the SEC is connected to the positive one of the rectifier bridge, whereas their negative terminals are connected directly. The diode provides a transmission channel for electrical power under low wind speeds. The switch status of this diode is determined by the voltage difference between both sides of the dc bus. The dc bus of the GCI is linked to the output dc bus of the DWIG directly without a booster device. Thus, the efficiency of the wind energy utilization is increased, and the hardware structure and control of the grid-connected operation are simplified.

Under low wind speeds, the output dc bus voltage of the rectifier bridge is too low to reach the given value even if the entire capacity of the SEC supplies the reactive excitation power. The voltage-boosting ability of the SEC is exploited to acquire a high dc voltage. Thus, the electrical power is supplied to the load through the dc bus of the SEC when the diode is on while the rectifier bridge on the power side is blocked.

The output voltage of the rectifier bridge increases with the rotor speed of the DWIG and the wind speed. Under a high wind speed, the diode is switched off once the output voltage of the rectifier bridge exceeds the dc bus voltage of the SEC. The electrical power is transferred from the rectifier bridge to the load, and the reactive power is provided by the SEC and ac excitation capacitors at that moment. Thus, a stable output dc voltage is achieved by adjusting the reactive power from the SEC under such working conditions. The volume and capacity of the SEC can be optimized by choosing a reasonable excitation capacitance. Moreover, the dc bus voltage of the SEC should be constant for the steady operation of the SEC.

The active power from the generator is transferred from the GCI to the grid, and the power factor is usually equal to 1. If compensation reactive power is required, the power factor can also be a different value. Maximum power tracking is accomplished with the common control schemes of the generator and inverter. Therefore, the combined system control strategy and the corresponding specific excitation capacitor optimization are important in this grid-connected wind power system.

The two sets of stator windings share the same rated dc bus output voltage. To achieve a satisfactory dynamic performance after the two sides of the dc bus are connected in parallel, the number of control-winding turns should be fewer than the number of power-winding turns. In this way, the voltage drop in the impedance of the filter inductance decreases. In other words, the terminal voltage of the control winding should be lower than that of the power winding.

III. Control Strategy For Grid-Connected DWIG Wind Turbine For Wide Speed Ranges

For the stable operation of the proposed grid-connected DWIG wind turbine, emphasis should be placed on a constant high dc voltage in a wide speed range. Such requirement eliminates the need for a booster converter for the GCI. IN addition, focus should be centered on realizing a grid-connected operation by using the integrated control of the generator and inverter while tracking the maximum power. Thus, the dc voltage control strategy, in which the active and reactive currents of the SEC are adjusted, and the cooperation control between the generator and the inverter are important elements in this system. These elements are included in the following control strategies for the grid-connected DWIG wind turbine.

A. Principle of Control-Winding-Voltage-Orientation Control Strategy and Instantaneous Power Theory

On the basis of instantaneous reactive power theory [17], [18], the instantaneous active power p and reactive power q are defined in (1) using the power invariance of the Park transformation and arbitrary reference coordinates.

$$\begin{cases} p = u_x i_x + u_y i_y \\ q = u_x i_y - u_y i_x \end{cases} \tag{1}$$

where u and i are the instantaneous voltage and current, respectively, for a three-phase circuit, and subscripts x and y represent the direct and quadrature axes for the arbitrary reference coordinates. For example, subscripts d and q are used in two-phase rotating reference coordinates. Similarly, for the stationary coordinate, the subscripts α and β are used. Thus, in (1), the values of p and q are independent of the defined reference coordinates.

From (1), if the instantaneous power and voltage are known, the corresponding current can be calculated as follows:

$$\begin{cases} i_x = \dfrac{p u_x - q u_y}{u_x^{\,2} + u_y^{\,2}} \\ i_y = \dfrac{p u_y + q u_x}{u_x^{\,2} + u_y^{\,2}} \end{cases} \tag{2}$$

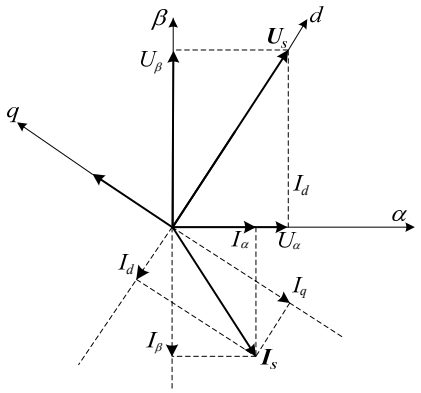

Fig. 2. Simplified diagram based on the control-winding terminal voltage orientation.

By replacing subscripts *x* and *y* in (2) with *d* and *q*, respectively, we obtain the corresponding current components for the *d-q* rotating reference coordinates.

$$\begin{cases} i_d = \dfrac{pu_d - qu_q}{u_d^{\,2} + u_q^{\,2}} = \dfrac{pu_d - qu_q}{|\boldsymbol{U}|^2} \\ i_q = \dfrac{pu_q + qu_d}{u_d^{\,2} + u_q^{\,2}} = \dfrac{pu_q + qu_d}{|\boldsymbol{U}|^2} \end{cases} \tag{3}$$

The *d-q* reference coordinate is oriented by the control-winding terminal voltage vector [16]. A simplified orientation diagram is shown in Fig. 2.

In this particular voltage-oriented reference frame, the voltage components of the *d* and *q* axes are described as follows:

$$\begin{cases} u_d = |\boldsymbol{U}| = |\boldsymbol{U}_s| \\ u_q = 0 \end{cases} \tag{4}$$

The abovementioned orientation method is extremely useful in analyzing the instantaneous active and reactive power. By substituting the current subscripts *x* and *y* with *d* and *q*, respectively, we can rewrite (2) as follows according to (4):

$$\begin{cases} i_d = \dfrac{p}{u_d} = \dfrac{p}{|\boldsymbol{U}_s|} \\ i_q = \dfrac{q}{u_d} = \dfrac{q}{|\boldsymbol{U}_s|} \end{cases} \tag{5}$$

Thus,

$$\frac{p}{q} = \frac{i_d}{i_q} \tag{6}$$

The q component of the control-winding current i_q obviously produces instantaneous reactive power q, whereas i_d generates p. In addition, electromagnetic torque T_{em} can be used to regulate the dc bus voltage U_{sDC} of the SEC, and the manipulation of T_{em} can be accomplished by controlling p. Moreover, q can adjust the control-winding flux and then change the internal magnetic field of the DWIG [8]. Hence, the power-winding terminal voltage U_{pDC} can be regulated by q. In conclusion, the control relationship can be summarized as follows:

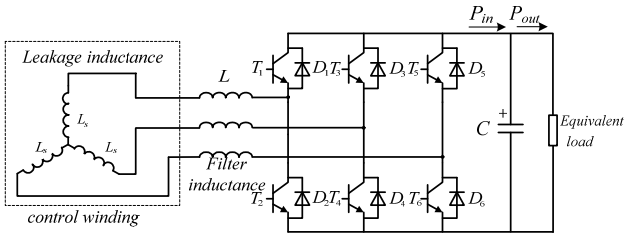

Fig. 3. Connection between the control winding and the SEC.

$$\begin{cases} i_d \to p \to T_{em} \to U_{sDC} \\ i_q \to q \to \Phi_m \to U_{pDC} \end{cases} \tag{7}$$

B. Voltage Control Strategy in Wide Wind Speed Range

1) Voltage Control Strategy under Low Wind Speed: Owing to the saturated flux caused by the excessive regulation of the dc bus voltage to reach the set value, a voltage booster function of the SEC on the control-winding side is employed to broaden the utilization of wind energy under a low wind speed. Under these circumstances, the parallel diode is on, and the electrical power is transferred from the dc bus of the SEC to the GCI.

To acquire a high dc voltage under a low wind speed, the voltage booster function of the SEC is exploited. As shown in Fig. 3, the control-winding leakage inductance and filter inductance are used to store electric energy. When zero vectors are chosen, the control windings are short-connected. Under this circumstance, the induced electro-motive forces (EMFs) serve as the power supply. As a result, the phase current and electric energy stored in the inductance both increase. When nonzero vectors are selected, the electric energy stored in the inductance is conveyed to the dc bus through an antiparallel diode. The continuous storage and release of electric energy in the inductance increases the dc bus voltage as long as the input active power to the filter capacitor P_{in} is greater than the output power P_{out}. The dc bus voltage rises or drops when P_{in} is greater or less than P_{out}. Thus, the closed-loop regulator of the dc bus voltage determines the duty cycle of the switching tubes. Given that the output active power variations do not induce reactive current changes in the SEC, the active power loss of the SEC and the output active power both determine the active current i_{sd}.

To improve the dynamic performance and load capacity of the DWIG at a low rotor speed, the magnetic flux of the DWIG should be kept constant. The induced EMF of the single-phase control winding can be expressed as

$$E_s = 4.44 f_1 N_s K_{ws} \Phi_m \tag{8}$$

where f_1, N_s, K_{ws}, and Φ_m are the synchronous frequency, number of turns in the control winding, the winding coefficient, and the main flux of the generator, respectively. Obviously, Φ_m should be maintained as a constant by regulating E_s under a variable rotor speed. However, controlling E_s directly is difficult. In fact, the voltage drop in the control-winding impedance can be ignored here because it is significantly lower than the induced EMF. Therefore, phase voltage U_s is approximately equal to E_s, and the main flux Φ_m can thus be adjusted by controlling U_s under a variable rotor speed. In this study, the amplitude of the control-winding voltage vector $|\boldsymbol{U}_s|$ is employed to regulate the flux Φ_m.

To ensure the constant slope of the curve $|\boldsymbol{U}_s|/f_1$ for regulating Φ_m, the reference value $|\boldsymbol{U}_s|^*$ depends on the synchronous frequency f_1 varying continuously with wind speed. The feedback value of $|\boldsymbol{U}_s|$ is calculated by using the sampled control-winding line voltage. Thus, the given reactive current i_{sq}^* is obtained from the PI regulator of $|\boldsymbol{U}_s|$. In addition, (7) shows that an increasing $|\boldsymbol{U}_s|$ contributes to a reduction in i_{sd} and i_{sq}, which results in the steady operation of the system.

2) Voltage Control Strategy under High Wind Speed: As soon as the dc bus voltage of the rectifier bridge on the power-winding side reaches the set value under a high wind speed, the parallel diode is turned off. The electrical power is transferred from the power-winding side. Equation (8) shows that the adjustment of the main flux Φ_m changes the single-phase winding voltage. Consequently, controlling the control-winding flux Φ_s can also regulate the output dc bus voltage $U_{p\mathrm{DC}}$ under different rotor speeds and loads for the same magnetic field shared by two sets of stator windings. Given that the reactive current from the excitation capacitor is non-adjustable, the controllable reactive current is provided mainly by the SEC, and the given i_{sq}^* can thus be obtained from the $U_{p\mathrm{DC}}$ regulator.

Although no active power is exported from the control-winding side, limited active losses, such as line resistor losses and switching losses, still exist. To guarantee the stability of the SEC, i_{sd} must be controlled to keep $U_{s\mathrm{DC}}$ steady in real time. The inputs of two dc bus voltage regulators are the differences between their respective dc bus voltage reference values and measured values.

3) Integrated Voltage Control Strategy for DWIG in a Wide Wind Speed Range: Although different active and reactive power control strategies for regulating output voltage are employed under low and high speeds, they can be merged into one type of integrated voltage control strategy. Only the given and feedback values of one voltage outer loop need to be changed. The feedback parameters are measured in real time to guarantee a soft switch between the two types of operational modes. The specific integrated voltage control strategy for a wide wind speed range is shown in Fig. 4. The switchover between the low wind speed and the high wind speed operation modes is determined by the rotor speed.

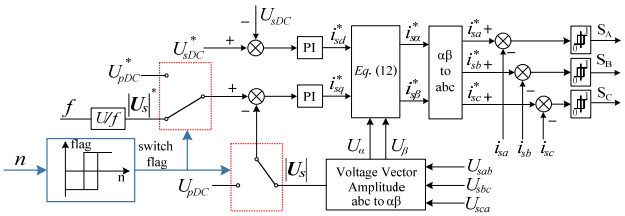

Fig. 4. Integrated voltage control strategy diagram of proposed DWIG wind power system.

i_{sd}^* and i_{sq}^* are calculated with their own outer regulator. Then, by substituting α and β for subscripts x and y in (2) and replacing d and q according to (5), we can express the reference values for the α-β stationary coordinates as

$$\begin{cases} i_\alpha^* = \dfrac{i_d^* u_\alpha - i_q^* u_\beta}{|\boldsymbol{U}_s|} \\ i_\beta^* = \dfrac{i_d^* u_\beta + i_q^* u_\alpha}{|\boldsymbol{U}_s|} \end{cases} \tag{9}$$

The references i_{sa}^*, i_{sb}^*, and i_{sc}^* are calculated through the stationary coordinate transformation from α-β into a-b-c. The ac-side voltage vector of the SEC is regulated by switch signals S_A, S_B, and S_C derived from a two-level current hysteresis comparator. The errors between the current references i_{sa}^*, i_{sb}^*, and i_{sc}^* and the measured currents i_{sa}, i_{sb}, and i_{sc} are regarded as inputs of the hysteresis comparator.

C. Control Strategy for Grid-Connected Inverter

A double closed-loop structure is usually applied in the control strategy for a conventional full-power GCI, such as that in PMSM wind turbines. The given active current is dependent on the fluctuation of the dc link voltage. Hence, the output of the outer-loop voltage regulator is regarded as the given input of the current inner loop. However, the GCI circuit in a DWIG wind power system is simplified so that a boost converter is not needed because the front-end DWIG outputs a stable, high dc bus voltage with a wide wind speed range. Therefore, the dc current fluctuates with the output power if the outer-loop voltage regulator is still applied in a grid-connected DWIG wind turbine.

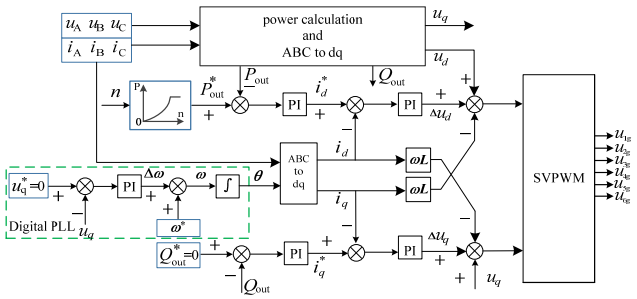

Fig. 5. Control schematic diagram of the GCI.

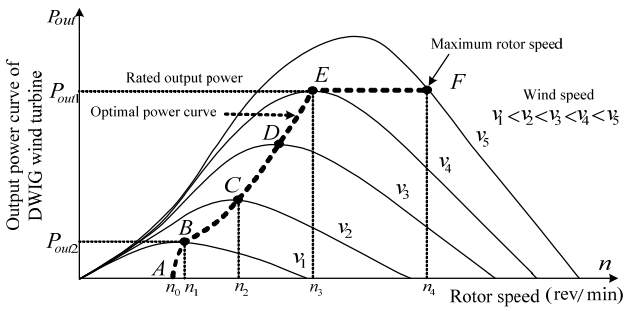

Fig. 6. Operational characteristics of DWIG wind power system under various wind speeds.

A special double closed-loop control scheme is proposed. The output of the outer-loop power regulator serves as the given reference of the current inner loop, and the set value of the power outer loop is derived from the optimal characteristic curve of the DWIG output power. The maximum power point tracking is fulfilled by the optimal output power characteristic and the received feedback output active power. Thus, the DWIG controller is obviously combined with an inverter controller, which embodies the control integrality of the proposed grid-connected wind turbine. The block diagram of the control strategy of the GCI is given in Fig. 5.

In decreasing the impact on the grid at the cutting-in moment, the output voltage vector from the GCI is regulated by a space voltage vector PWM to follow the grid-side voltage. At the initial time, the given active power is 0. The feedback current and voltage components from the grid side play a key role in balancing and overcoming slight fluctuations. The voltage-orientation angle used in the calculation of coordinate transformation is obtained from the digital phase locking loop (PLL), which is implemented by a closed-loop control of the network-side voltage reactive component.

The controllable characteristic of reactive power aids the DWIG wind turbine in providing support to the grid during grid faults. The proposed control strategy for GCIs can also contribute to the improvement of the grid-fault ride-through ability of DWIG wind turbines. Although the output power fluctuates at twice the power grid frequency during asymmetric grid faults, only the dc bus current fluctuation at twice the power grid frequency exists in the DWIG wind power system. Thus, the dynamic performance of the DWIG is not affected by such a load current fluctuation.

D. Operational Characteristics of DWIG Wind Power System under Various Wind Speeds

Depending on the optimal power curve of the wind turbine, different running states, and the corresponding output power in a wide wind speed range, the operation of a grid-connected DWIG wind power system can be divided into four main stages. As shown in Fig. 6, the process from the initial generation to the maximum rotor speed operation occurs in four stages.

1) Stage I: The start-up stage is shown in the A-B section in Fig. 6. After the wind speed reaches the start-up speed, the vanes start to rotate, and the rotor speed of the DWIG increases gradually. As the DWIG is not switched to the power generation mode at this moment, the DWIG has no electrical energy output.

2) Stage II: The voltage build-up stage is shown in the B point in Fig. 6. As the rotor speed of the DWIG reaches a set minimum value, the DWIG begins to build up voltage. In this process, the reactive power is provided both by the excitation capacitors and the SEC. To guarantee the normal operation of the SEC, the dc bus voltage of the SEC should be regulated to be stable by compensating for the active power loss of the SEC. After this short process, the DWIG enters the power generation state.

3) Stage III: The low wind speed operation stage is shown in the B-C section in Fig. 6. When the wind speed reaches the cut-in speed, the system begins to transfer electric power to the GCI from the dc bus of the SEC. A high dc voltage is acquired by the voltage booster function of the SEC. The magnetic flux of the DWIG is regulated to maintain a constant less-than-rated value and thereby improve the dynamic performance and load capacity of the DWIG. As the show in the B-C section in Fig. 6, the current magnitude of the SEC is mainly determined by the output active power.

4) Stage IV: The high wind speed operation stage is shown in the C-D-E-F section in Fig. 6. The electric power is transferred from the dc bus of the rectifier bridge to the inverter. The adjustable reactive power from the SEC is provided to keep the output dc voltage stable, and the adjustable active power keeps the dc bus voltage of the SEC steady. In this stage, the excitation current magnitude of the SEC depends mainly on the reactive power because the active loss of the SEC is relatively small. The E-F section is regarded as the flux weakening control region, and the output active power is maintained at a constant value. The C-D-E section shows no difference for the control strategy, but the excitation reactive current is too excessive to be extracted by the SEC.

IV. Optimization Scheme of Excitation Capacitor for a Wide Wind Speed Range

The proposed grid-connected DWIG wind power system is different from previous systems [8], [11]. The control strategy applied under two working conditions leads to different active power flow directions. Consequently, the composition and proportion of the control-winding current are distinct. The active current is the major component of the control-winding current under low wind speeds, whereas the reactive component is the primary component under high wind speeds. Hence the influence generated by various excitation capacitors on the control-winding current is also different from that of previous systems. Therefore, the capacity optimization scheme for the SEC that is suitable for this proposed grid-connected DWIG wind power system should be investigated.

A. Control-Winding Current under Low Wind Speed

The excitation reactive current provided by the SEC merely maintains Φ_m constant under low wind speeds, whereas the active current increases along with the active power output. Thus, the active current occupies the leading position in the control-winding current. To simplify our analysis, the influence of mutual leakage between two sets of stator windings is ignored, and only the fundamental component is taken into consideration. The excitation reactive current fed from the SEC to adjust Φ_m is regarded as a current source [11]. The simplified equivalent circuit of the DWIG wind power system with a resistance load operating under a low wind speed is shown in Fig. 7 (a), and the corresponding phasor diagram is shown in Fig. 7 (b).

According to Kirchhoff's circuit laws, the relationship of the current phasors in Fig. 7 (a) is expressed as

$$\dot{I}_m = \dot{I}_r + \dot{I}_s + \dot{I}_p \tag{10}$$

where $\dot{I}_m$ is the excitation reactive current fed from the SEC and the subscripts r, s, and p express the equivalent rotor winding, control winding, and power winding, respectively.

The amplitude of $\dot{I}_m$ can be derived from the phasor diagram.

$$I_m = I_{sC} + I_p\cos\beta - I_L\sin\gamma - I_r\sin\alpha \tag{11}$$

where I_{sC} and I_L are the reactive component and active component of the control-winding current. As shown in Fig. 7 (b), all the unknown parameters in (11) can be expressed as follows:

$$\cos\beta = \frac{U_p - I_p X_p}{E_m},\ \sin\gamma = \frac{I_L X_s + I_{sc} R_s}{E_m},\ \sin\alpha = \frac{I_r X_r}{E_m},$$

$$I_p = U_P\cdot\omega C,\quad I_r = \frac{E_m^2}{\sqrt{(\frac{R_r}{s})^2 + X_r^2}},\quad I_m = \frac{E_m}{X_m}.$$

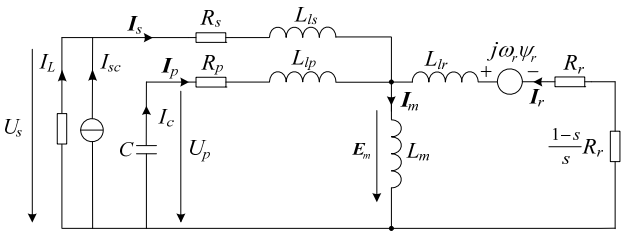

(a) Equivalent circuit.

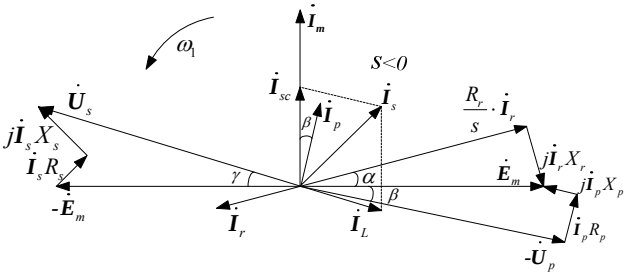

(b) Phasor diagram.

Fig. 7. Equivalent circuit and phasor diagram of the DWIG operating under a low wind speed.

Thus, the reactive component of the control-winding current used to adjust the magnetic flux under a low wind speed is described as follows:

$$I_{sC} = \frac{E_m}{E_m + I_L R_s}\left\{\frac{E_m}{X_m} + \frac{E_m X_r}{(\frac{R_r}{s})^2 + X_r^2} - U_P\omega C\cdot\frac{U_p - U_P\omega C R_p}{E_m}\right\} - \frac{I_L^2 X_s}{E_m + I_L R_s} \tag{12}$$

Thus, the magnitude of the control-winding current can be calculated by

$$I_s = \sqrt{I_{sC}^2 + I_L^2} \tag{13}$$

In the generation mode, the slip ratio s is negative and can be given as follows [8], [11]:

$$s = \frac{-3E_m^2 R_r + \sqrt{9E_m^4 R_r^2 - 4P_e^2 R_r^2 X_r^2}}{2P_e X_r^2} \tag{14}$$

Here, P_e is the electromagnetic power transferred from the rotor to the stator. The control-winding current under different rotor speeds and output power can be determined from (12)-(14).

The above derivation processes and derivation results reveal that the amplitude and phase of the control-winding current depend on the excitation capacitor and output active power (represented by I_L) under low wind speeds. Obviously, I_L plays a decisive role in the control-winding current when operating under a low wind speed.

B. Control-Winding Current under High Wind Speed

Under a high wind speed, the active component in I_s

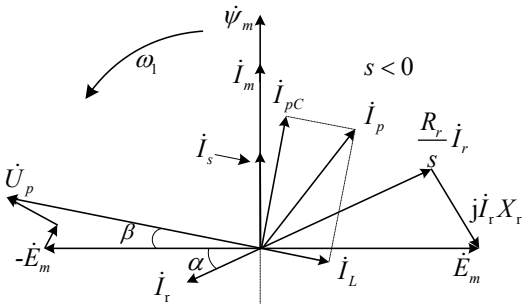

Fig. 8. Phasor diagram of the DWIG operating under a high wind speed.

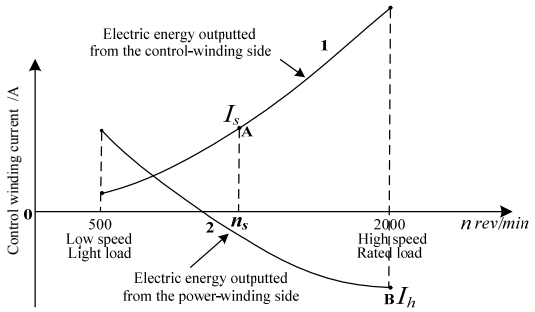

Fig. 9. Change of control-winding current in different wind speed zones.

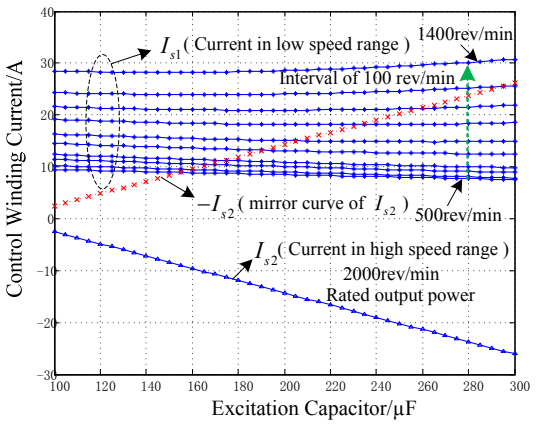

Fig. 10. Influence of excitation capacitor on control-winding current.

can be ignored because the active power loss of the SEC is small. Hence, the phase of I_s stays the same as that of or becomes the opposite of I_m if the loss is ignored. The control-winding current can also be regarded as a current source. As wind speed increases, the reactive excitation power provided by the excitation capacitor is excessive, and the SEC extracts this part of the excitation power. The adjustable reactive excitation power supported by the SEC can guarantee a stable dc output voltage.

According to [10], the value of I_s is described as

$$I_s = \frac{E_m}{X_m} + \frac{E_m X_r}{\left(\frac{R_r}{s}\right)^2 + X_r^2} + \frac{I_p^2 R_L - U_p^2 \omega C}{E_m} \quad (15)$$

where R_L represents the equivalent load. The expression of the slip ratio s is the same as that in the low-speed operation mode. The excitation current supplied by the SEC in the high-speed operation mode can be obtained from (15). The phase diagram for the DWIG operating under a high wind speed is displayed in Fig. 8.

C. Optimal Scheme of Excitation Capacitor

The variations in the control-winding current for two different working statuses are shown in Fig. 9. The two curves indicate the variation in the control-winding current when electric energy is transferred from the control-winding side or the power-winding side in a wide wind speed range from 500 rev/min to 2,000 rev/min. Curve 1 in Fig. 9 shows the variation in the control-winding current in low-speed mode, and the value of I_s is always positive. Curve 2 in Fig. 9 indicates the variation in the control-winding current in high-speed mode, and the value of I_s becomes negative when the reactive excitation current provided by the excitation capacitor is excessive. The rotor speed n_s represents the switchover speed between the two operation modes.

The maximum positive control-winding current under a low wind speed appears at the switch point (point A in Fig. 9), and the minimal negative current I_h under a high wind speed appears at a high-speed rated load time (point B in Fig. 9). Therefore, the effect of the switchover speed must be considered in this optimization problem. If the condition $|I_s| = |I_h|$ is satisfied, then an appropriate excitation capacitor under variable speed and load is determined. In other words, the minimal capacity of the SEC for the proposed grid-connected DWIG wind power system is obtained.

D. Optimization Results

To further adjust the optimal value of the excitation capacitor, we construct a simulation model for the proposed DWIG wind power generation system using MATLAB/Simulink as our platform. Some parameters of the DWIG prototype are given in Appendix A.

The influences exerted by various excitation capacitors on the control-winding current I_s under the two different operation modes are investigated. The simulation results are shown in Fig. 10. The control-winding current in the low-speed range is denoted as I_{s1}, and the simulation results for the control-winding current with a variable excitation capacitance value per 100 rev/min interval are all given. I_{s2} is the control-winding current with a full load under a maximum rotor speed of 2,000 rev/min. $-I_{s2}$ is the mirror curve of I_{s2}. The intersection point between I_{s1} and $-I_{s2}$

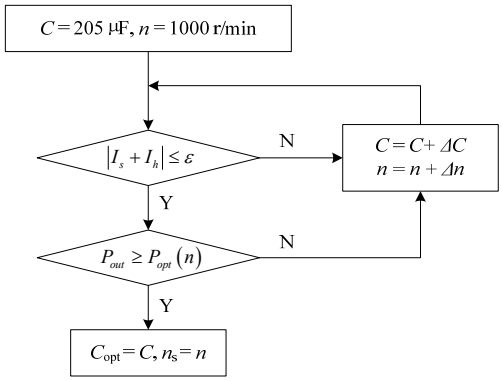

Fig. 11. Process of optimal approximation for excitation capacitance and switch speed.

is where the condition $|I_s| = |I_h|$ is met. As shown in Fig. 10, the amplitude of I_s undergoes minimal change as the excitation capacitance varies in a low-speed situation, but it does depend on the output active power. On the contrary, I_s is closely related to the excitation capacitance value in high-speed situations.

As the DWIG prototype is designed to output a voltage of 600 V at 1,000 rev/min, the switchover speed between the two operation modes should exceed 1,000 rev/min. Therefore, a switchover rotor speed of 1,000 rev/min and the corresponding excitation capacitance of 205 μF (the intersection between I_{s1} and $-I_{s2}$ at 1,000 rev/min) are chosen as the initial conditions for the following optimal approximation, as shown in Fig. 11. $P_{opt}(n)$ is the optimal output power for the different rotor speeds of the generator. The increment of the excitation capacitance and rotor speed are 5 μF and 20 rev/min, respectively.

After a comprehensive analysis of this simulation, an optimal excitation capacitance of 235 μF and a switchover rotor speed of 1,100 rev/min are obtained. To avoid frequent switching between the two operation modes, a hysteresis comparison of rotor speeds is employed to assess and execute the switching between the two control strategies. The hysteresis width is set to 50 rev/min.

E. Simulation Results

After the optimization procedure is completed, the simulation verification for the whole DWIG wind power generation system is carried out. The integrated voltage control strategy presented in Section VIII is applied in this simulation model, and the excitation capacitance of 235 μF and switchover rotor speed of 1,100 rev/min are selected. The output power of the DWIG is determined with the optimal power characteristic curve. The corresponding simulation results are shown in Fig. 12. To facilitate the implementation and control, the amplitude of the control-side voltage vector $|\boldsymbol{U}_s|$ used in low-speed mode is replaced with U_{pDC}. As the

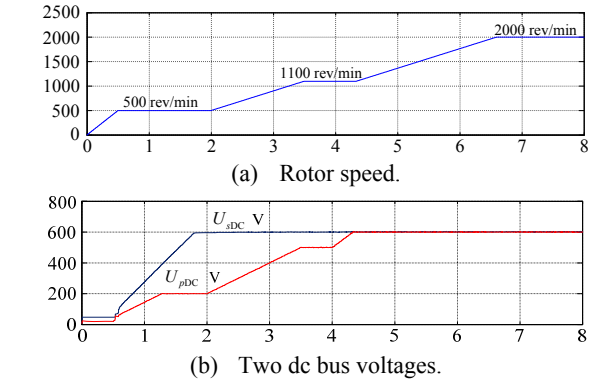

(a) Rotor speed.

(b) Two dc bus voltages.

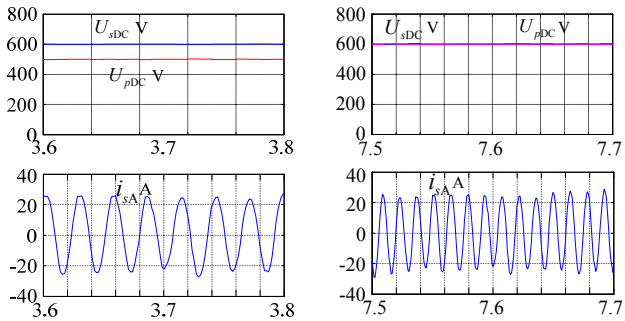

(c) Two dc bus voltages and phase current of control winding in 3.6–3.8 s at 1,100 rev/min.

(d) Two dc bus voltages and phase current of control winding in 7.5–7.6 s at 2,000 rev/min.

Fig. 12. Simulation results of the proposed grid-connected DIWG wind power system based on the optimal capacitor.

two stator windings share the same magnetic field, the two quantities share a turn ratio relationship. Thus, this simplified method is still used in the subsequent experimental verification (the feedback and control voltage U_{pDC} are both labeled as $|\boldsymbol{U}_s|$).

As shown in Figs. 12 (a) and (b), when the rotor speed reaches the initial rotor speed of 500 rev/min at 0.5 s, the DWIG begins to build up voltage. The two dc bus voltages U_{pDC} and U_{sDC} gradually increase to the given values of 600 and 200 V and then remain nearly unchanged. At this moment, the system runs under a low-speed operation mode. The rotor speed starts to rise at a constant speed after 2 s. The set value of U_{pDC} changes linearly from 200 V to 500 V under the low-speed operation mode, and the given value of U_{sDC} is always 600 V. When the rotor speed exceeds the switchover speed of 1,100 rev/min, the electrical power is diverted to transfer from the rectifier bridge on the power side. This state transition happens at 4 s. Thereafter, the working stage reaches the high-speed operation mode. The rotor speed increases from 1,100 rev/min to 2,000 rev/min and remains at such level. Both dc bus voltages can be regulated to maintain their level at 600 V during this process.

The detailed simulation results of the dc bus voltages and

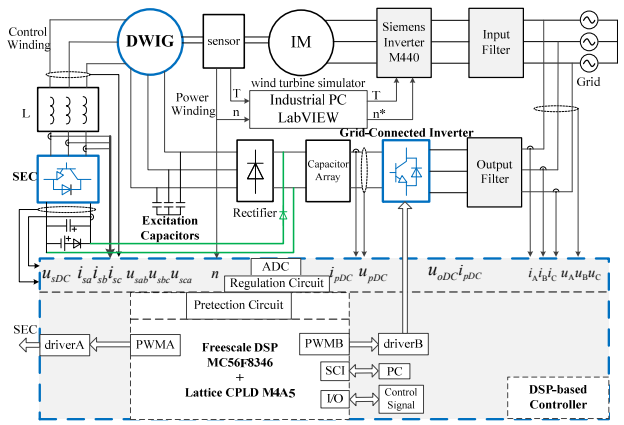

Fig. 13. Experimental prototype of proposed grid-connected DWIG wind power system.

phase current of control winding at the switchover speed of 1,100 rev/min and maximum speed of 2,000 rev/min are shown in Figs. 12 (c) and (d). The RMS values of the control-winding phase current in the two processes are both 18 A approximately. Therefore, the chosen optimal capacitor can obviously realize the capacity minimization of the SEC for the proposed grid-connected DWIG wind power system. The correctness of the simulation results is verified by the following experiments.

V. Experimental Verification

A 37 kW/600 V prototype of the grid-connected DWIG wind power system is developed to carry out an experiment, as shown in Fig. 13.

The GCI is designed for a rated power of 50 kW. The main circuits of the SEC and GCI are composed of three-leg Mitsubishi intelligent power modules. The entire control strategy is implemented in a Freescale MC56F8346 digital signal controller, which exhibits two independent PWM interfaces suitable for controlling the SEC and GCI simultaneously. The prime mover is simulated by a three-phase induction motor driven by a Siemens M440 inverter. An industrial PC with the LabVIEW software is employed to control the M440 inverter, simulate wind-turbine characteristics, and track wind energy. The parameters of this prototype are shown in Appendix A.

To achieve a complete experimental verification of the proposed grid-connected DWIG wind power system, we divide the experiment into four parts: low wind speed status, high wind speed status, grid-connected operating mode, and excitation capacitor optimization.

A. Experimental Results under Low Wind Speed

The DWIG begins to build up voltage when the speed exceeds the minimum value of 500 rev/min. The in-service wind turbine blade determines the building-up rotor speed in practical applications. The experimental waveforms during this process are shown in Fig. 14. After the initial excitation generated by the 48 V battery, the dc bus voltage is built up reliably and stably. No overshoots in voltage or current waveforms occur. The dc bus voltage of the SEC successfully remains stable at 600 V. The amplitude of the control-side voltage vector $|\boldsymbol{U}_s|$, which represents reactive power, is maintained at a given value of 200 V.

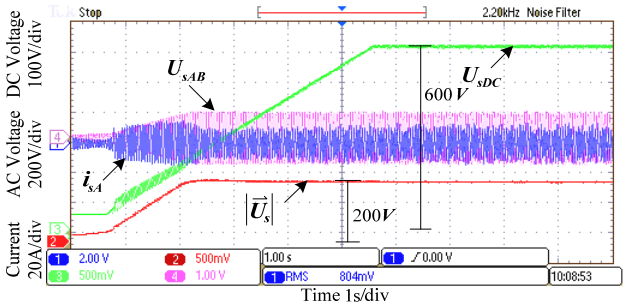

Fig. 14. Voltage and current waveforms during the process of building up voltage at 500 rev/min.

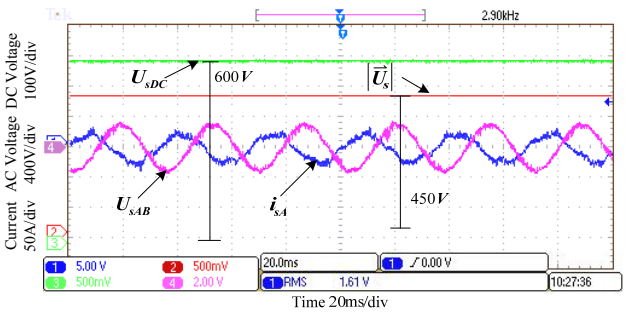

Fig. 15. Voltage and current waveforms when outputting 8 -kW active power at 1,000 rev/min.

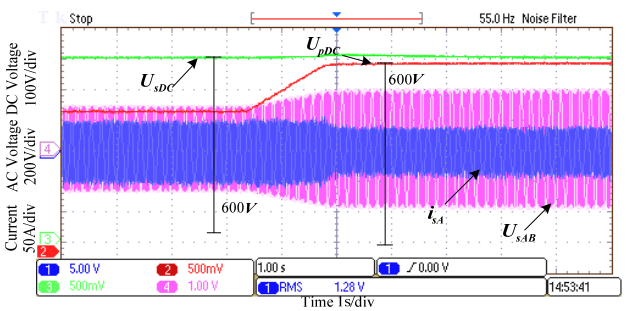

Fig. 16. Voltage and current waveforms during switching from low wind speed mode to high wind speed mode.

Fig. 15 presents the voltage and current waveforms of the DWIG at 1,000 rev/min when outputting 8 kW of active power. The results prove that the dc bus voltage and amplitude of the control-winding voltage vector are regulated to be steady at given values. The system runs steadily in the low-speed operation mode. In Fig. 14, u_{sab} is the control-winding line voltage of phases a to b and i_{sa} is the control-winding current of phase a. The definitions of the other variables are the same as those in the sections above.

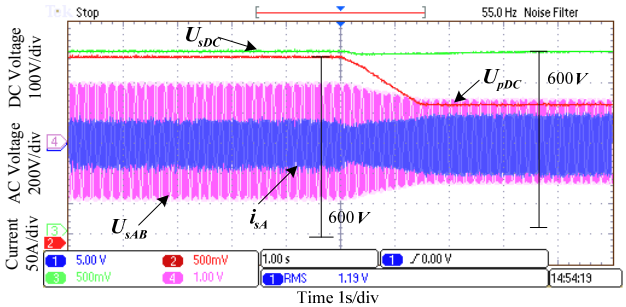

Fig. 17. Voltage and current waveforms during switching from high wind speed mode to low wind speed mode.

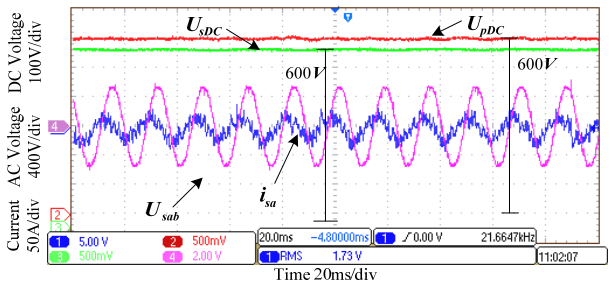

Fig. 18. Voltage and current waveforms during the output rated at 37 kW at 2,000 rev/min.

As the rotor speed reaches the predetermined switchover rotor speed of 1,100 rev/min, the switchover flag changes to "1". After the power-side dc bus voltage increases smoothly to the given value of 600 V, the parallel diode enters the off state. The electrical power is diverted to transfer from the rectifier bridge. The dc bus voltage of the SEC is kept at the set value of 600 V throughout the transition process without any fluctuations, and the output dc voltage is maintained at a stable level by controlling the reactive power of the system. Fig. 16 shows the voltage and current waveforms of this system during switching from low wind speed mode to high wind speed mode.

B. Experimental Results under High Wind Speed

To avoid frequent switching between two operating situations, the switchover speed from the high wind speed mode to the low wind speed mode is defined as 1,050 rev/min. The voltage and current waveforms during switching from the high wind speed mode to the low wind speed mode are shown in Fig. 17. During the transition process, the control-winding dc bus voltage drops to less than 20 V to achieve a rapid change in the two dc bus currents.

The voltage and current waveforms operating at the maximum rotor speed of 2,000 rev/min in high wind speed mode are exhibited in Fig. 18. The excess reactive power supplied by the excitation capacitor to the generator is extracted by the SEC. The line current leads the line voltage at the phase position. The dc bus voltages at both winding sides are regulated to small-scope fluctuations at the given value.

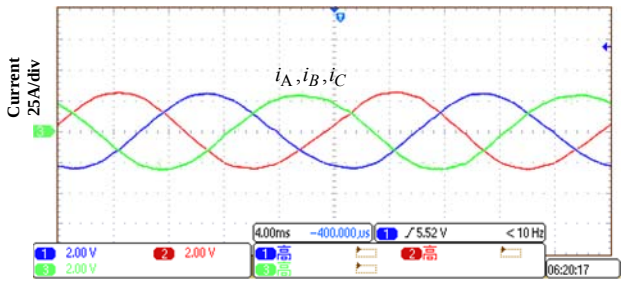

(a) Three-phase current waveforms.

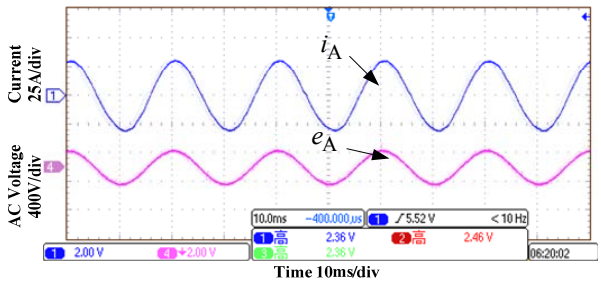

(b) Single-phase voltage and current waveforms.

Fig. 19. Voltage and current waveforms of the GCI during the output of 11 kW of active power.

C. Experimental Results for Grid-connected Inverter

The three-phase current waveform and single-phase voltage and current waveforms for the GCI during output at 11 kW of active power are displayed in Fig. 19. Low harmonic content and high power factor are obviously achieved. This result demonstrates the accuracy of the proposed double closed-loop control strategy and the robustness of the GCI without a boost converter.

D. Experimental Results for Optimization of Excitation Capacitor

To prove the accuracy of the optimization scheme for the excitation capacitor, we perform several experiments at different wind speeds. The goal is to measure the control-winding current from the start of the build-up of the rotor speed at 500 rev/min to the maximum rotor speed of 2,000 rev/min (100 rev/min). The relationship of the output active power and control-winding current RMS value under different rotor speeds is shown in Fig. 20 (negative RMS value means opposite current direction). The maximum RMS value occurs at the switchover speed and the maximum speed. Their corresponding voltage and current waveforms are shown in Figs. 21 and 18, respectively.

The experimental results reveal that the RMS value of the control-winding current increases with a rise in rotor speed during low wind speed mode. Once the rotor speed is higher than the switchover speed, the control-winding current becomes negative during the high wind speed mode. Moreover, the RMS value of the control-winding current also rises with the enhancement of the rotor speed in high wind speed mode. The minimal negative current almost equals the

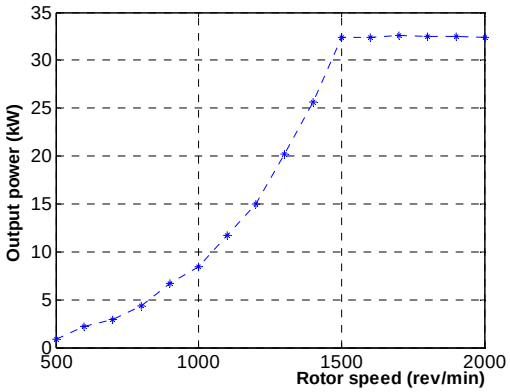

(a) Output power.

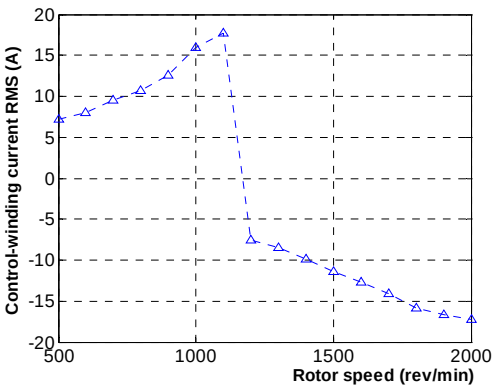

(b) Control-winding current RMS.

Fig. 20. Experimental results for output power and control-winding current RMS from 500 rev/min to 2,000 rev/min.

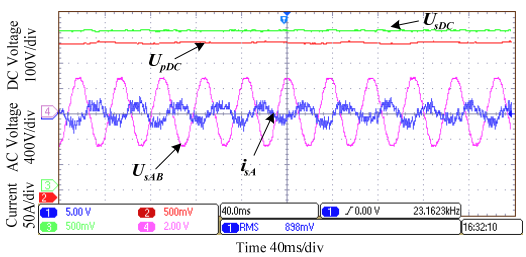

Fig. 21. Voltage and current waveforms during 12 kW output at 1,100 rev/min.

maximum positive current, and the minimal current value is approximately 18 A. The results are consistent with the theoretical analysis and simulation results and thereby demonstrate the accuracy of the proposed optimization scheme for excitation capacitors. The maximum capacity of the SEC is only one-third of the rated output power. No additional cost is involved for greater wind energy utilization in the rotor speed range of 1:4.

VI. Conclusion

A grid-connected DWIG wind power system for wide wind speed ranges is proposed. A parallel connection topology between two stator-winding sides is employed to broaden the utilization capability of wind energy at a low wind speed. The integrated voltage control strategies help the DWIG in output a stable high dc voltage in a wider wind speed range than before (a rotor speed range of 1:4 in this work). Given that an extra boost converter is not needed, the circuit structure and control strategy of the GCI are both simplified.

By combining the control of the generator and GCI, the grid-connected DWIG wind turbine runs stably and exhibits good operational performance. To decrease the volume and capacity of the SEC, we propose an appropriate excitation capacitor optimization scheme considering the active and reactive current composition of proportions in different operation modes and meeting the requirements of tracking maximum power. The volume and capacity of the SEC is only one-third of the rated output power. Therefore, a wider scope for wind energy utilization, smaller volume and capacity of the SEC, and a simpler GCI circuit and control without a boost converter make the grid-connected DWIG wind power system more competitive than other wind turbines. In addition, the high-quality dynamic performance of the proposed system in outputting a stable, high dc voltage allows the grid-connected DWIG wind turbine to ride through grid faults easily. This topic is our next key research work.

Appendix

The following are the parameters of the designed DWIG (both the rotor and control windings are converted to a power winding):

$R_p = 0.78\,\Omega$; $R'_s = 0.535\,\Omega$; $R'_r = 0.384\,\Omega$;

$L_{lp} = 5.84$ mH ; $L'_{lr} = 2.86$ mH ; $L'_{ls} = 4.38$ mH ;

$L_m = 165.5$ mH ; $L_{ps} = 0.57$ mH ;

Turns ratio: $N_s : N_p = 52 : 60$;

Rated power: 37 kW;
Rated speed: 1,500 rev/min;
Maximum speed: 2,000 rev/min;
Pole pairs: 2;
Rated dc output voltage: 600 V;
Filter inductor: 3×4 mH ;
Excitation capacitor: $3 \times 235\,\mu$F ;
DC bus capacitor: $1100\,\mu$F / 900 V ;
Voltage of battery: 48 V.

The designed parameters for the GCI are as follows:
Rated power: 50 kW;
Filter inductor: 3×4 mH ;
Voltage on grid side: 155 V;
DC bus capacitor array: 17 mF / 900 V .

Acknowledgment

This work was supported in part by the National Natural Science Foundation of China under Award No. 51407085,

the Postdoctoral Science Foundation of China under Award No. 2015M571685, the Fundamental Research Funds for the Central Universities under Grant NJ20160046, the grant from the Priority Academic Program Development of Jiangsu Higher Education Institution and Jiangsu University Senior Talents Special Project under award 13JDG111.

REFERENCES

[1] H. Li, and Z. Chen, "Overview of different wind generator systems and their comparisons," *IET Renewable Power Generation*, Vol. 2, No. 2, pp. 123-138, Jun. 2008.

[2] A. C. Smith, R. Todd, M. Barnes, and P. J. Tavner, "Improved energy conversion for doubly fed wind generators," *IEEE Trans. Ind. Appl.*, Vol. 42, No. 6, pp. 1421-1428, Nov./Dec. 2006.

[3] R. C. Bansal, T. S. Bhatti, and D. P. Kothari, "Bibliography on the application of induction generators in non- conventional energy systems," *IEEE Trans. Energy Convers.*, Vol. 18, No. 3, pp. 433-439, Sep. 2003.

[4] E. Touti, R. Pusca, J. Manata, J. Brudny, and A. Chaari, "On the use of a dimmer for a robust frequency control of a self-excited three-phase induction wind generator," *Journal of Power Electronics*, Vol. 14, No. 3, pp. 580-591, May 2014.

[5] O. Ojo and I. E. Davidson, "A dual stator winding induction generator with a four switch inverter-battery scheme for control," in *Proc. IEEE PESC,* pp. 230-234, Galway, Jun. 2000.

[6] O. Ojo and I. E. Davidson, "PWM-VSI inverter-assisted stand-alone dual stator winding induction generator," *IEEE Trans. Ind. Appl.*, Vol. 36, No. 6, pp. 1604-1611, Nov. 2000.

[7] D. Wang, W. Ma, F. Xiao, B. Zhang, D. Liu, and A. Hu, "A novel stand-alone dual stator-winding induction generator with static excitation regulation," *IEEE Tran ㄴ. Ind. Appl.*, Vol. 20, No. 4, pp. 826-835, Dec. 2005.

[8] Y. Li, Y. Hu, W. Huang, L. Liu, and Y. Zhang, "The capacity optimization for the static excitation controller of the dual-stator-winding induction generator operating in a wide speed range," *IEEE Trans. Ind. Electron.*, Vol. 56, No. 2, pp. 530-541, Feb. 2009.

[9] N. M. Kirby, L. Xu, M. Luckett, and W. Siepmann, "HVDC transmission for large offshore wind farms," *Power Engineering Journal*, Vol. 16, No. 3, pp. 135-141, Jul. 2002.

[10] P. Bresesti, W. L. Kling, R. L. Hendriks, and R. Vailati, "HVDC connection of offshore wind farms to the transmission system," *IEEE Trans. Energy Convers.*, Vol. 22, No. 1, pp. 37-43, Mar. 2007.

[11] F. Bu, W. Huang, Y. Hu, and K. Shi, "An excitation-capacitor-optimized dual stator-winding induction generator with the static excitation controller for wind energy application," *IEEE Trans. Energy Convers.*, Vol. 26, No. 1, pp. 122-131, Mar. 2011.

[12] K. Shi, W. Huang, Y. Hu, and F. Bu, "An indirect-field-oriented dual stator-winding induction generator for the wind power system applications," in *Proc. WNWEC,* pp. 152-156, 2009.

[13] D. Wang, W. Ma, and Y. Guo, "Optimal design of a self-excited capacitor in a dual-stator winding induction generator," *IET Electric Power Appl.*, Vol. 3, No. 4, pp. 334-342, Jul. 2009.

[14] A. M. Knight and G. E. Peters, "Simple wind energy controller for an expanded operating range," *IEEE Trans. Energy Convers.*, Vol. 20, No. 2, pp. 459-466, Jul. 2005.

[15] E. Koutroulis, and K. Kalaitzakis, "Design of a maximum power tracking system for wind-energy-conversion applications," *IEEE Trans. Ind. Electron.*, Vol. 53, No. 2, pp. 486-494, Apr. 2006.

[16] F. Bu, Y. Hu, W. Huang, S. Zhuang, and K. Shi, "Wide-speed-range-operation dual stator-winding induction generator DC generating system for wind power applications," *IEEE Trans. Ind. Electron.*, Vol. 30, No. 2, pp. 561-573, Mar. 2015.

[17] T. Furuhashi, S. Okuma, and Y. Uchikawa, "A study on the theory of instantaneous reactive power," *IEEE Trans. Ind. Electron.*, Vol. 37, No. 1, pp. 86-90, Mar. 1990.

[18] F. Z. Peng and J. Lai, "Generalized instantaneous reactive power theory for three-phase power systems," *IEEE Trans. Instrum. Meas.*, Vol. 45, No. 1, pp. 293-297, Feb. 1996.

Kai Shi was born in Suzhou, China, in 1980. He received his B.S. degree in Automation and his M.S. degree in Power Electronic and Power Transmission from Jiangsu University, Zhenjiang, China, in 2002 and 2005, respectively. He received his Ph.D. degree in Power Electronic and Power Transmission from Nanjing University of Aeronautics and Astronautics, Nanjing, China, in 2012. Since 2002, he has been with the School of Electrical and Information Engineering, Jiangsu University. Since 2013, he has been an Assistant Professor in Jiangsu University. His current research interests include wind power generator control, grid-connected control, and control strategies of low-voltage ride through.

Peifeng Xu was born in Nantong, China, in 1980. She received his B.S. and M.S. degrees in Electrical Engineering from Jiangsu University, Zhenjiang, China, in 2002 and 2005, respectively. Since 2002, she has been working at the School of Electrical and Information Engineering, Jiangsu University, Zhenjiang, China. Since 2007, she has been a Lecturer at Jiangsu University. Her current research interests include the design and control of high-efficiency wind power generators.

Zenqiang Wan was born in Nantong, China, in 1991. He received his B.S. degree in Electrical Engineering from Jiangsu University, Zhenjiang, China, in 2014. Since 2014, he has been a graduate student at the School of Electrical and Information Engineering, Jiangsu University, Zhenjiang, China. His current research interests include the grid-connected control of high-efficiency wind power generators and low-voltage ride-through control.

Feifei Bu was born in Maanshan, Anhui Province, China in 1984. He received the B.S. degree in the Electrical Engineering from Anhui University of Technology, Maanshan, China, in 2006. In 2014, he joined the faculty of the College of Automation Engineering, NUAA, where he is currently a Lecturer. His main research interests include stand-alone

power systems, wind power systems, control and optimal design for generator systems and variable-speed drives.

Zhiming Fang was born in Zhenjiang, China, in 1978. He received his M.S. degree in Control Theory and Control Engineering from Jiangsu University, Zhenjiang, China, in 2003. He received his Ph.D. degree in Control Theory and Control Engineering from Nanjing University of Science and Technology, Nanjing, China, in 2012. Since 2000, he has been a Faculty Member of Jiangsu University, where he is currently a lecturer. His main research interests include switched systems, nonlinear control, robust control, and parallel robot control.

Rongke Liu was born in Changzhou, China, in 1977. He received his B.S. degree in Mechanical Engineering from Southwest Traffic University, Chengdu, China, in 2000. Since 2003, he has been a Senior Engineer at KTK Group, Changzhou, China. His main research interests include the mechanical design and integrated design of power supply systems.

Dean Zhao was born in Changzhou, China, in 1956. He received his B.S. degree in Industrial Electric Automation and his M.S. degree in Machine Manufacturing from Jiangsu University, Zhenjiang, China, in 1982 and 1989, respectively. He received his Ph.D. degree in Power Electronic and Power Transmission from Nanjing University of Aeronautics and Astronautics, Nanjing, China, in 2007. Since 2000, he has been a Professor at the School of Electrical and Information Engineering, Jiangsu University. He is currently an Academic Leader in Agriculture Electrification and Automation, Jiangsu University. His current research interests include the production process research of intelligent automation and network control, the computer intelligent control, and robot control.